Did increased flooding during the African Humid Period force migration of modern humans from the Nile Valley?

Abdallah S. Zaki, Georgina E. King, Negar Haghipour, Robert Giegengack, Stephen E. Watkins, Sanjeev Gupta, Mathieu Schuster, Hossam Khairy, Salah Ahmed, Mostafa El-Wakil, et al.

Quaternary Science Reviews 272 (2021) 107200

Contents lists available at ScienceDirect

Quaternary Science Reviews

journal homepage: www.elsevier.com/locate/quascirev

Did increased flooding during the African Humid Period force migration of modern humans from the Nile Valley?

Abdallah S. Zaki [a, *], Georgina E. King [b], Negar Haghipour [c, d], Robert Giegengack [e], Stephen E. Watkins [a], Sanjeev Gupta [f], Mathieu Schuster [g], Hossam Khairy [h], Salah Ahmed [h], Mostafa El-Wakil [h], Saleh A. Eltayeb [i], Frédéric Herman [b], Sébastien Castelltort [a]

[a] Department of Earth Sciences, University of Geneva, Geneva, Switzerland
[b] Institute of Earth Surface Dynamics, University of Lausanne, Lausanne, Switzerland
[c] Geological Institute, ETH Zürich, Zürich, Switzerland
[d] Laboratory of Ion Beam Physics, ETH Zürich, Zürich, Switzerland
[e] Department of Earth & Environmental Science, University of Pennsylvania, Philadelphia, USA
[f] Department of Earth Sciences and Engineering, Imperial College London, London, UK
[g] Université de Strasbourg, CNRS, Institut Terre et Environnement de Strasbourg, UMR 7063, 5 rue Descartes, Strasbourg, F-67084, France
[h] Egyptian Mineral Resources Authority (EMRA), Cairo, Egypt
[i] Department of Geology, University of Aswan, Aswan, Egypt

ARTICLE INFO

Article history:
Received 19 April 2021
Received in revised form
14 September 2021
Accepted 18 September 2021
Available online 14 October 2021

Handling Editor: Giovanni Zanchetta

Keywords:
Sahara
African humid period
Inverted channel
Human migration
Quaternary climate
Fluvial ridges

ABSTRACT

During the Quaternary period, the eastern Sahara's hydroclimate oscillated between wet and dry intervals. These oscillations caused drastic changes in precipitation rates, often associated with ancient human migrations. In particular, significant migration of riparian populations from the Nile Valley to the west and northwestward of the Sahara occurred during the African Humid Period (AHP), an episode of increased monsoons, which characterized North Africa in response to increasing insolation. Several fossil rivers, now preserved as ridges throughout southern Egypt due to their floodplains' deflation, contain archeological artifacts and thus represent a potentially important record of fluvial activity during this episode of past human dynamics and environmental change. Here we present ^{14}C and Optically Stimulated Luminescence (OSL) ages of sediments preserved in these palaeorivers, which cluster within the AHP and are thus consistent with increased fluvial activity during this distinct humid period. Palaeohydraulic reconstructions based on grain size, channel geometry, and drainage area suggest typical precipitation intensities of 55–80 mm/h during sediment transport events. Given previous annual rainfall estimates, these hydrologic conditions may have lasted, or occurred, during the AHP up to 3–4 times more frequently than before and after this period. Such intense fluvial activity is consistent with monsoon intensification and may have rendered the area inhospitable for human settlements, congruent with population migration out of the Nile Valley during the AHP. These findings highlight links between past human ecodynamics and environmental signals, providing a concrete narrative of human population response to warming with potential echo in the current situation.

1. Introduction

Late Quaternary climate oscillations in the eastern Sahara region have been identified, based on palaeo-discharge and sediment-load estimates of the Nile River, cave speleothems, dust fluxes, pollen records, groundwater-fed deposits, ancient watercourses, archeological evidence, and abrupt fluctuations of lake levels and lacustrine deposits (Fig. 1A; Foucault and Stanley, 1989; Hoelzmann et al., 2000; Schuster et al., 2005; Hamdan and Brook, 2015; Hoffmann et al., 2016; Drake et al., 2011; Williams et al., 2015; Macklin et al., 2013, 2015; Woodward et al., 2015; Abotalib et al., 2016; Palchan and Torfstien, 2019; Manning and Timpson, 2014;

* Corresponding author. Department of Earth Sciences, University of Geneva, Rue des Maraîchers 13, 1205, Geneva, Switzerland.
E-mail address: Abdallah.zaki@etu.unige.ch (A.S. Zaki).

https://doi.org/10.1016/j.quascirev.2021.107200

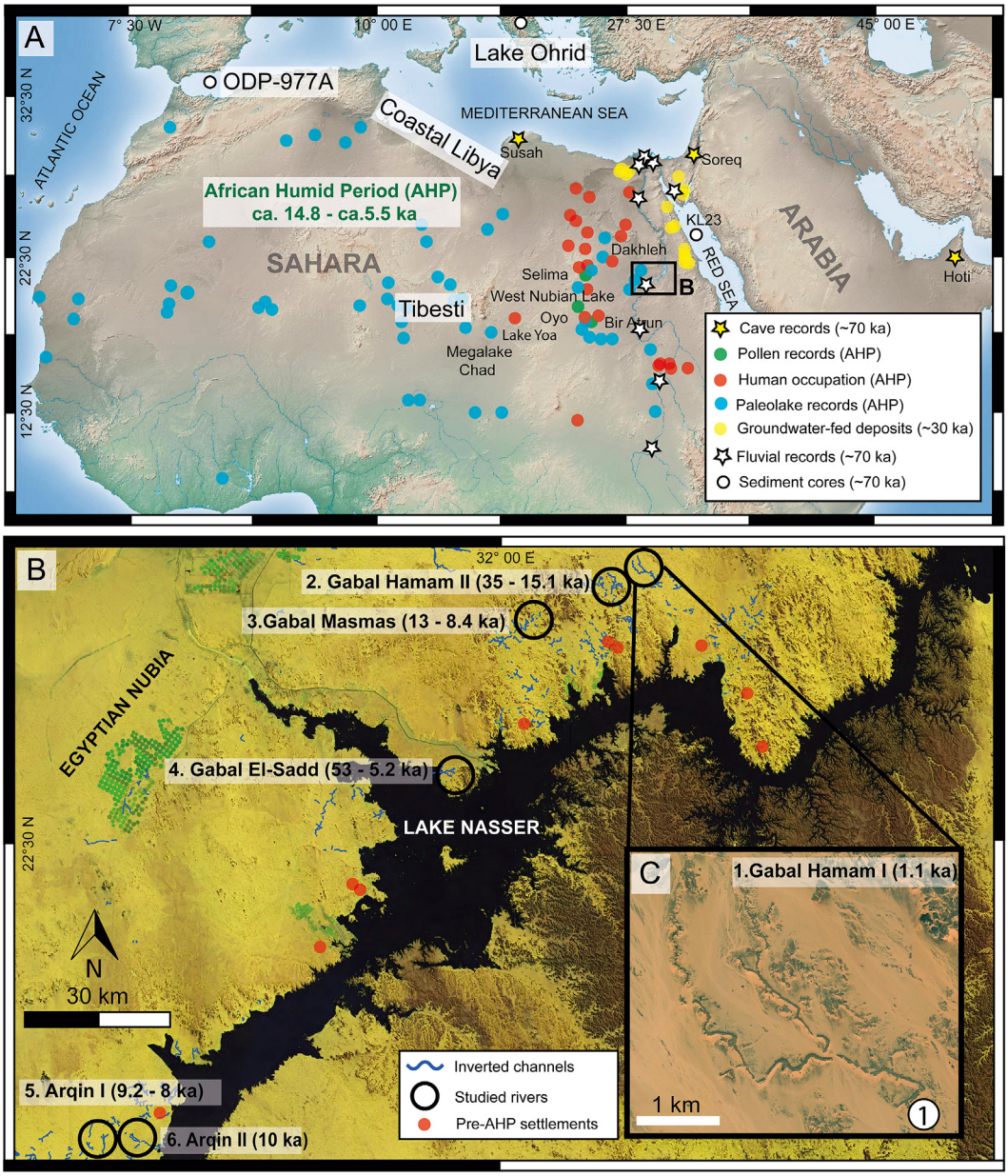

Fig. 1. (A) The distribution of climatic proxies that indicate humid phases over the past ~70 ka, particularly the African Humid Period (AHP): pollen records (Ritchie and Haynes, 1987; Haynes et al., 1989), human occupation in the eastern Sahara (Kuper and Kröpelin, 2006), lacustrine deposits (Hoelzmann et al., 2000; Schuster et al., 2005; Ritchie and Haynes, 1987; Haynes et al., 1989, Damnati, 2000; Kröpelin et al., 2008), groundwater-fed deposits (Hamdan and Brook, 2015; Hamdan and Lucarini, 2013; Abotalib et al., 2016), cave speleothems (Hoffmann et al., 2016; Fleitmann et al., 2011; Bar-Matthews et al., 2003), sediment cores (Palchan and Torfstien, 2019; Martrat et al., 2004; Wagner et al., 2019), and fluvial records (Macklin et al., 2015; Williams et al., 2015; Abotalib et al., 2019). (B) Digitally rendered mosaic of Landsat 8 image relief map showing the location of the study area and the distribution of the ancient rivers in southern Egypt. (C) Portion derived from Esri World Imagery shows Gabal Hamam I palaeo-river standing as ridges in the modern landscape.

Pausata et al., 2020). These proxies suggest that at least four humid periods may have punctuated the past ca. 65 ka. The last and most significant wet period, based on the interpretation of archeological sites associated with palaeo-zoological proxies and pollen records (Ritchie and Haynes, 1987; Haynes et al., 1989; Kuper and Kröpelin, 2006; deMenocal et al., 2000), persisted from early to mid-Holocene time, and was termed the "African Humid Period" (AHP; ca.14.8 - ca.5.5 ka BP, deMenocal et al., 2000). Although a number of uncertainties remain on the regional extent of this wet period across North Africa, as well as on its timing and magnitude (see Williams, 2019a, 2019b, pp. 105–106; Woodward et al., 2015), notably because of evidence of low lake and river discharge levels during this period (Gasse et al., 2008; and review in Williams, 2019a, 2019b, pp. 107–126), multiple palaeo-climatic proxies nevertheless broadly converge toward estimates of annual precipitation rates of 300–920 mm/yr in the eastern Sahara (Ritchie and Haynes, 1987; Hoelzmann et al., 2000; Tierney et al., 2017). This humidity favored the growth of vegetation, the multiplication of active rivers and the development of perennial lakes, turning the arid Sahara into a savannah-like environment, and may have made the Nile Valley into a marshy and hazardous place, which is hypothesized to have triggered the migration of its riparian populations toward the deep Sahara across several hundreds of kilometers (Kuper and Kröpelin, 2006). To further test how

plausible the hypothesis is that environmental perturbations during the AHP drove human migration away from the Nile Valley, this work aims to estimate the palaeo-rainfall intensities involved in transforming the Nile Valley into an inhospitable region.

To do this, we reconstruct palaeo-rainfall rates from a spectacular set of six fossil river deposits (now expressed as sinuous ridges of fluvial sediments in the modern landscapes in response to differential erosion, Zaki et al., 2021) in the eastern Sahara (Fig. 1B and C). The presence of these palaeo-rivers implies prior wetter conditions across a broad swath of the present-day desert of southern Egypt and thus is a witness of the transition from past humid conditions to the current hyper-arid environment. The archeological content of these fossil river deposits (lithic artifacts and pottery shards, Zaki and Giegengack, 2016; Giegengack and Zaki, 2017; Zaki et al., 2018) suggests that the rivers were active during Mid-Pleistocene to Holocene time. Here we present the first inferred geochronological constraints on these river systems. When coupled with estimates of precipitation from palaeo-hydraulic reconstructions and calculated sedimentation rates, our study enables a quantitative assessment of rainfall perturbations during late-Quaternary climate oscillations in the Sahara, particularly during the AHP. Our results have major implications for human occupation patterns in the region during the Holocene and provide a perspective from the past relevant to modern environmental change.

2. Materials and methods

The six studied palaeo-rivers form sinuous, single-thread channel-fill planforms, expressed as sinuous ridges in the present-day landscape, and are distributed across ~38,000 km^2 of southern Egypt and northern Sudan (Fig. 1 B–C; Zaki and Giegengack, 2016; Giegengack and Zaki, 2017). We used satellite imagery to trace and map the source to the sink of those palaeo-rivers. A few sinks are now submerged beneath the water of Lake Nasser. We, therefore, used the CORONA satellite images that were captured before the complete filling of Lake Nasser.

Inverted channels' geometry could be measured from the field or aerial and satellite images, as they stand as hills rather than troughs (Williams et al., 2009). Here we measured the palaeochannel geometries of the six rivers from the field to avoid significant uncertainty—the obtained channel widths from the field range from 30.5 to 65.5 m (Table S1). To constrain the palaeochannel height, we measured the thickness of the preserved material in the palaeochannel fill. The preserved material consists of highly cemented sandy gravels. Due to possible original channel-fill incomplete preservation, we used 35% as uncertainty, as it has been previously suggested (Paola and Borgman, 1991) that the preserved thickness compared to the actual mean depth is around 60–70%. In this study, the measured channel thickness of the six rivers ranges from 0.75 to 1.2 m (Table S1). To determine the median grain size distribution (D_{50}) of these palaeo-channels, we measured the b-axes of between 100 and 127 clasts (>2 mm), which were randomly selected from an area of 1 m^2 based on established methods (Table S1; Wolman, 1954; Chen et al., 2018; Duller et al., 2012).

The discovery of palaeolithic and pottery sherds in the sedimentary fill of a palaeochannel indicates that these palaeo-rivers were active during the Middle Pleistocene and Holocene epochs (Zaki and Giegengack, 2016; Giegengack and Zaki, 2017). We, therefore, collected nine samples for OSL dating from sandy/gravel beds of three palaeo-rivers, where forcing a plastic tube into a cleaned outcrop surface was possible (Table S 1). Six samples of fluvial sediments were collected for ^{14}C dating from the other three palaeo-rivers that were characterized by highly cemented gravels, with insufficient fine material for OSL (Table S 1).

Samples for OSL dating were prepared using standard methods under subdued red light at the University of Lausanne, Switzerland. Following removal of material that may have been exposed to light during sampling, samples were extracted from the sampling tubes and treated with HCl and H_2O_2 to remove carbonates and organic material, respectively. The samples were then sieved to extract the 180–212 μm fraction before being treated with heavy liquids to isolate the K-feldspar rich (<2.58 g cm^{-3}) and quartz-rich (2.58–2.65 g cm^{-3}) components. The quartz-rich fraction was then treated with concentrated HF to remove contaminating feldspars and also the alpha irradiated exterior of the grains. An untreated part of the bulk sample was also dried to determine the sample water content, and a fraction of this material was prepared for ICP-MS analysis to determine the U, Th, and K concentrations for environmental dose rate determination.

Environmental dose rates were calculated using DRAC (v.1.2; Durcan et al., 2015) with the conversion factors of (Guerin et al., 2011) and using the grain size attenuation factors of (Mejdahl, 1979; Bell, 1980). For feldspar grains, the internal K-content was assumed to be 12.5 ± 0.5% after (Huntley and Brail, 1997), and an a-value of 0.15 ± 0.05 was used after (Balescu et al., 2003). The cosmic dose rate was calculated following (Prescott and Hutton, 1994). The calculated environmental dose rates are summarised in Table S2. All luminescence measurements were made at the University of Lausanne. The protocol used in the age measurements and uncertainties has been used in detail in the Supplementary Materials (Tables S2–S3).

Radiocarbon dating was performed on total organic carbon (TOC) extracted from sediment samples collected from 3 palaeo-rivers. The samples were fumigated in silver capsules (Elementar) with HCl (37%) to remove carbonate (Komada et al., 2008) and neutralized for 48 h at 65 °C using solid NaOH to remove residual acid. The samples were wrapped in a tinfoil boat (Elementar) and pressed prior to analysis. Fumigated samples were measured as gas targets using MICADAS system at ETH-Zurich (Table S4). Samples were normalized using oxalic acid II (NISTSRM4990C), and they were corrected for constant contamination introduced during fumigation and capsules contribution. The radiocarbon dates were calibrated with the calibration curve IntCal13 (Reimer et al., 2013) using the OxCal v. 4.2 software (Bronk Ramsey, 2009).

For palaeo-hydraulic reconstructions, we used the palaeo-slope equation (Trampush et al., 2014):

$$\log S = \alpha_0 + \alpha_1 \log D_{50} + \alpha_2 \log H_{bf} \quad (1)$$

where S is river slope, D_{50} is median grain size, (H_{bf}) is channel depth, and α0, α1, and α2 are empirical coefficients with values of −2.08 ± 0.0015, 0.254 ± 0.0007, and −1.09 ± 0.0019 respectively. We combined (Eq. (1)) with Manning's equation (Eq. (2)) to calculate palaeo-flow velocity (U):

$$U = 1/n\,(R^{2/3} S^{1/2}) \quad (2)$$

where (U) is flow velocity (m/s), (n) is Manning's coefficient (n = 0.03 ± 0.005), and (R) is the hydraulic radius, approximated by channel height. Flow velocity is then multiplied by channel depth and width to obtain volumetric water discharge Q_w (m^3/s).

To estimate each river's palaeodrainage area (A), we used the current topography and drainage area above each sampling site (flow routing algorithm on 25m resolution PALSAR DEM data), assuming the modern topography has remained mostly unchanged through late Quaternary arid climate and low erosion rates. We cross-validated those estimates using Hack's law of drainage area

and length (L) for individual drainage networks (Hack, 1957; Sassolas-Serrayet et al., 2018):

$$L = 1.4\,A^{0.6} \quad (6)$$

Although the absolute volume of rainfall cannot be estimated from fossil river deposits because the duration of channel-forming events is beyond dating resolution, an assessment of the rate of precipitation can be provided by dividing volumetric discharge by drainage area (constrained empirically and from DEMs). The rainfall rate is then expressed in millimeters per hour for the sake of comparison with modern rainfall rates. Hourly rates represent a close approximation of the intermittent nature of precipitation (Trenberth et al., 2017). In addition, a 1-h persistence of rainfall is considered representative of the typical duration of a storm that causes flood events over fast-responding (small) catchment areas (Brookes and Stensrud, 2000). In order to calculate the return period of estimated rainfall intensities before, during, and after the AHP, we compiled ~70 ka rainfall data derived from modeling in Tibesti and Coastal Libya (Blanchet et al., 2021), Lake Ohrid (Wagner et al., 2019), and pollen and palaeolake records in the eastern Sahara (Hoelzmann et al., 2000; Ritchie and Haynes, 1987; Haynes et al., 1989).

Clausius-Clapeyron (CC) scaling shows the relationship between precipitation and temperature change, supported by hourly, daily, and yearly data on rainfall globally (Trenberth et al., 2003; Lenderink and Meijgaard, 2008; Berg et al., 2013). The scale principally describes that an increase in temperature of one degree enhances the atmosphere's water-holding capacity at a rate of 7% (Trenberth et al., 2003). During the AHP, there was an increase of 7.5 °C in sea surface temperature in the Alboran Sea due to the transition from glacial to an interglacial period (Martrat et al., 2004). Factoring for the 7.5 °C temperature increase of the AHP would enhance the holding-water capacity by ~66%. So-called "super" Clausius-Clapeyron have been invoked to describe temperature-driven increase in rainfall in excess of "normal" CC: above threshold temperature of 12 °C, the atmosphere's water-holding capacity increases by 14% for each additional degree.

3. Results

The six palaeo-rivers, now expressed as resistant ridges (positive relief) in the modern landscape, consist of gravels accumulated in palaeo-channels, which do not exceed 1.2 m in height and display a maximum width of 65.5 m (Figs. 2 and 3; Table S1). We reconstructed the trajectory of these six palaeo-rivers (based on tributary structure) and found that five of them drained into the Nile River. Only one (Gabal El-Sadd palaeo-river) debouched into a vast plain, forming a fluvial fan that is now submerged by the water of Lake Nasser (Fig. 4). The gravel deposits are poorly sorted; clasts are angular to rounded in shape, with a median grain size (D_{50}) ranging from 26 ± 2 mm to 60 ± 3 mm; the sediment is mainly cemented by iron oxide. The deposits are massive, but pebble imbrications and a few cross-stratifications suggest conditions of unidirectional flow and bedload transport during channel-filling events.

New age constraints obtained via OSL and ^{14}C on channel-fill material indicate that the six palaeo-river systems in the southern Egyptian Sahara were active throughout the last ca. 53 ka (Fig. 5; 6A). Ages span from ca. 53 ± 7 ka BP to ca. 1.1 ± 0.25 ka BP. The oldest OSL ages are obtained at Gabal El-Sadd and Gabal Hamam II (Fig. 5), with ages of 53 ± 7 BP and ca. 35 ± 4 ka BP, respectively. At Gabal Hamam II, the 35 ka sediments are overlain by deposits that yield OSL ages of 16 ± 3 and 15.1 ± 4 ka BP. Although physical evidence of a stratigraphic break is not apparent, the abrupt superposition of ages in this section shows a probable period of erosion and/or non-deposition.

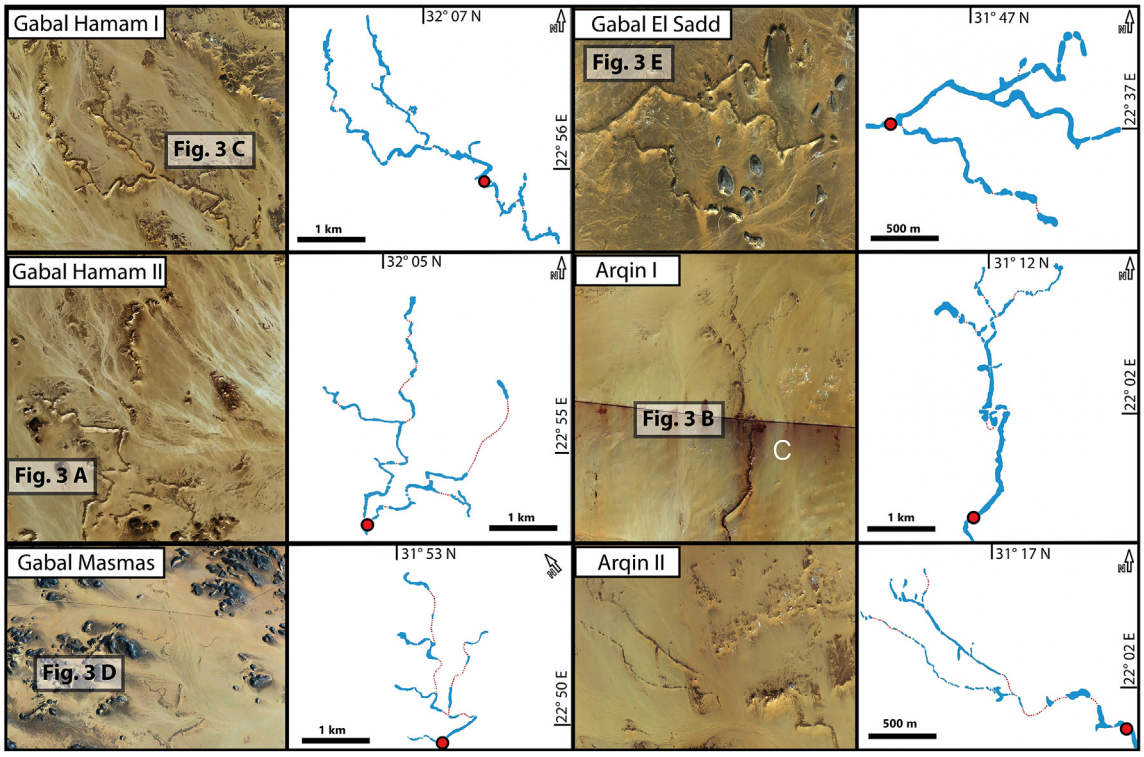

Fig. 2. Satellite images (ESRI World Imagery) and drawing of the reconstructed fluvial systems with an indication of each sampling site (red dots). (For interpretation of the references to colour in this figure legend, the reader is referred to the Web version of this article.)

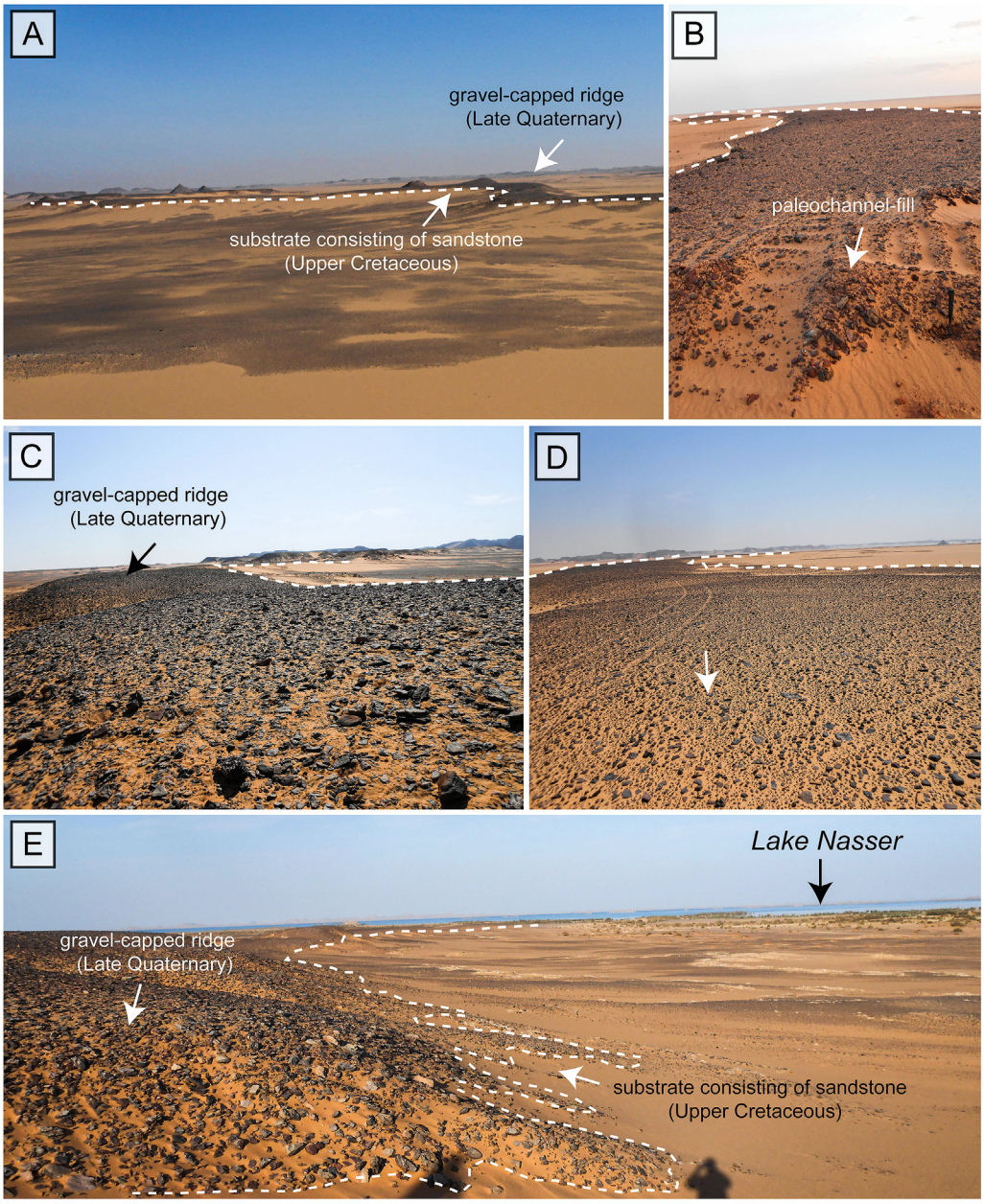

Fig. 3. Field photographs of ridges preserving a former rivers; (A) Gabal Hamam, (B) Arqin I, (C) Gabal Hamam I, (D) Gabal Masmas, and (E) Gabal El Sadd. The ridges typically comprise two stratigraphic units; the upper unit is gravel deposited during the Late Quaternary, and the lower unit consists of sandstone accumulated during the Upper Cretaceous epoch.

Palaeoriver deposits at Gabal Masmas, Arqin I, Arqin II, and Gabal El-Sadd yielded seven fluvial sediment OSL ages clustered between 13 ± 0.1 ka BP and 5.2 ± 1 ka BP (Fig. 5; Fig. 6A). This suggests a distinct episode of enhanced fluvial activity that transported and deposited sediments within the palaeo-river systems during this time interval, which corresponds to the AHP. Lack of fluvial sediment ages after 5 ka suggests that termination of the AHP likely occurred at ca. 5 ka before the present. However, two depositional ages in the Gabal El Sadd and Gabal Hamam I palaeo-rivers at 3.9 ± 0.7 BP ka and 1 ± 0.25 ka BP suggest that the past 5 ka were locally interrupted by fluvial activity. Further sampling in the upper part of our sections would be needed to confirm this hypothesis.

The measured channel heights range from 0.75 ± 0.26 m to 1.2 ± 0.42 m. We considered an average of 35% underestimation of channel depth to account for incomplete preservation of the original channel height (Paola and Borgman, 1991), and we evaluated uncertainties and dispersion using Gaussian error propagation. By coupling channel depth with grain-size distribution (D_{50}), we find that reconstructed fluvial palaeoslopes range from 0.003 ± 0.0012 to 0.0048 ± 0.0018, with a mean of 0.0037 ± 0.0014. Equilibrium flow velocities on such slopes obtained using (Eq. (2)), combined with channel heights and widths, indicate volumetric water discharge of 43 ± 16 to 138 ± 53 m^3s^{-1}. Estimated drainage areas of these palaeo-rivers are in the range of ca. 2.2 – ca.11.6 km^2 (Fig. S1). Given the estimated discharge, such drainage areas imply mean

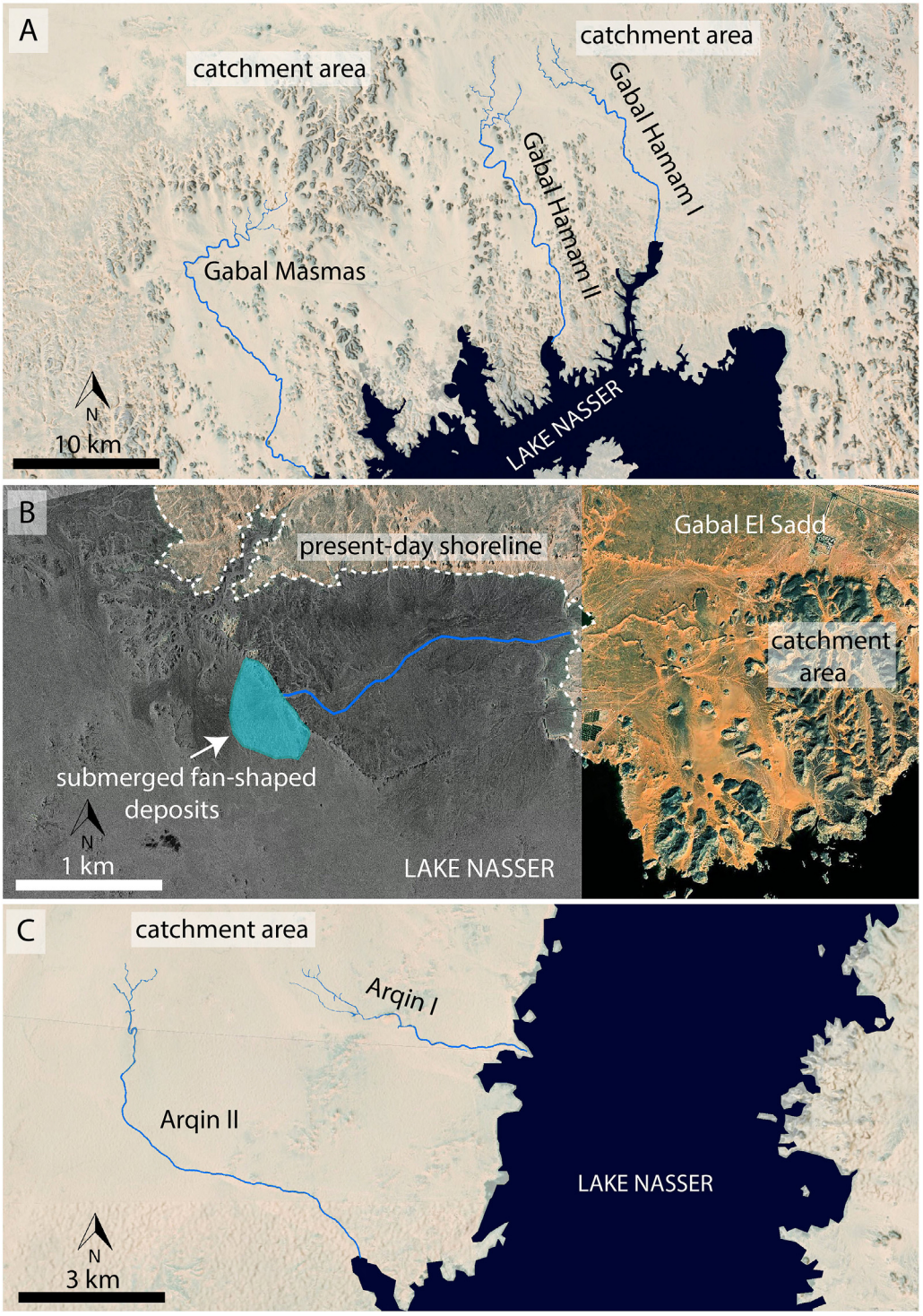

Fig. 4. Satellite images and line drawings of palaeo-rivers studied in this work; (A) Gabal Hamam I, Gabal Hamam II, and Gabal Masmas, (B) Gabal El Sadd, and (C) Arqin I, and Arqin II. These rivers were draining into the Nile River except for the Gabal El Sadd palaeo-river that debouched into a plain, forming a fan-shaped deposit. The fan is now submerged beneath the water of Lake Nasser. The rivers were mapped from Esri World Imagery, Google Earth imagery, CORONA images.

hourly rainfall rates in the range of 55–80 ± 26 mm/h; these intensities classify as heavy rainfall (American Meteorological Society, 2012). The small drainage areas (modern rivers with similar bankfull discharges usually have larger drainage areas, ranging from 80 to 900 km^2; Church and Rood, 1983; Trampush et al., 2014; Fig. S2), coupled with the discharge estimates, also reflect the high intensity of surface-runoff conditions that prevailed during the rainfall events.

Preserved age-thickness relationships indicate faster sedimentation rates during the early to mid-Holocene pluvial period than during other pluvial periods (Fig. 5). The Gabal Masmas, Arqin I, and Arqin II palaeo-rivers indicate 0.15 m–0.35 m of sedimentation in

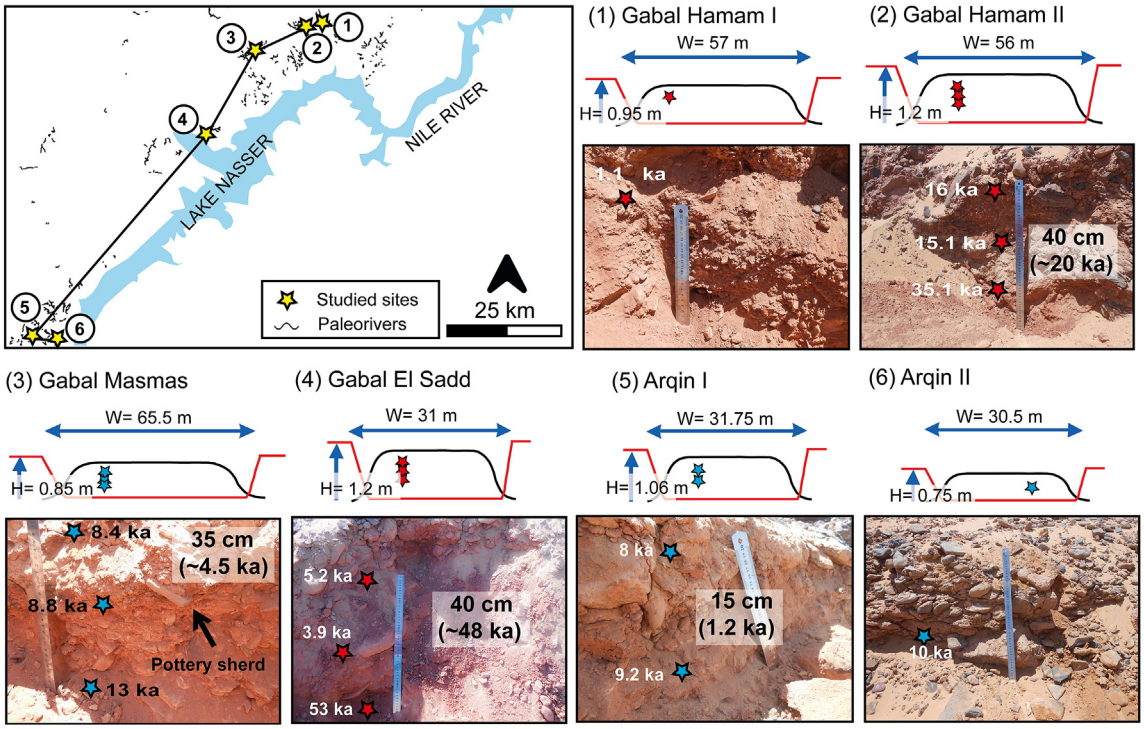

Fig. 5. Location map and field photographs of the studied sites with channel geometries (width and height), and datations points (OSL in red, and BP calibrated ^{14}C in blue). Channels do not exceed 1.2 m in height and 65.5 m in width, and consist of poorly sorted pebbles. The ages of fluvial activity cluster between 13 and 5.2 ka BP, which corresponds to the African Humid Period (AHP). (For interpretation of the references to colour in this figure legend, the reader is referred to the Web version of this article.)

ca. 1.2 and ca. 4.6 ka, respectively, during early to mid-Holocene time. In contrast, the Gabal El-Sadd and Gabal Hamam II palaeorivers record 0.4 m and 0.35 m of fluvial deposition in ca. 48 ka and ca. 20 ka, respectively (Fig. 5).

4. Discussion

Southern Egypt's fossilized rivers provide a unique archive of fluvial activity throughout the late Pleistocene and Holocene during the transition from past Saharan humid intervals to the present hyperarid conditions. Our data reveal six phases of sediment transport and deposition (Fig. 6A), which coincide with humid, cold, and arid conditions (e.g., Hoelzmann et al., 2000; Hamdan and Brook, 2015; Kleindienst et al., 2016; Ritchie and Haynes, 1987; deMenocal et al., 2000; Collins et al., 2013; Nicoll, 2004). Fluvial activity at 53 ka BP, 35 ka BP, and 13–5.2 ka BP took place in predominantly humid environments (Fig. 6A). Conversely, fluvial activity recorded at 15 ka BP, 4 ka BP, and 1 ka BP is likely associated with a cooler climate during Heinrich Stadial 1 (HS1; ca. 15 ka) and to the arid-hyperarid conditions of the past 4.5 ka (Collins et al., 2013; Nicoll, 2004). Nevertheless, the most significant cluster of ages obtained between 13 ± 0.1 ka BP and 5.2 ± 1 ka BP suggests a major episode of fluvial activity during the AHP, which represents an important constraint on current knowledge of environmental conditions during the AHP (Fig. 6A). This significantly more humid period is commonly explained by an astronomically driven increase of insolation that led to higher temperatures, increased rainfall, and lower dust fluxes, altogether enhancing vegetation diversification and human occupation of a more habitable deep Sahara (Fig. 6B and C; Palchan and Torfstien, 2019; Drake et al., 2011; Berger and Loutre, 1991; deMenocal et al., 2000; Martrat et al., 2004). This period ended between middle to late Holocene time when the region became more arid at ca. 5 ka; that aridity gradually intensified due to weaker insolation parameters (deMenocal et al., 2000; Nicoll, 2004). Mid-late Holocene aridification after the AHP was interrupted by briefly wetter conditions documented in northeastern Sudan at ca. 2 ka BP (Mawson and Williams, 1984) and supported by the two fluvial activity episodes recorded here at 4 ka BP and 1 ka BP. However, more recently, Macklin et al. (2013, 2015) reported two major episodes of channel contraction due to decreased Nile flows in northern Sudan between ca. 4–3 ka BP and after 3 ka BP (Fig. 6C). This suggests that these brief wet conditions may not have lasted for a prolonged period since significant channel contractions have been recorded in north Sudan (Macklin et al., 2013, 2015).

Before the AHP, modeled mean annual precipitation (MAP) rates range between less than ~50–~250 mm/yr (Fig. 6B). In contrast, during the AHP, palynological, geological, and biological proxies all suggest a much higher MAP range of ~300–920 mm/yr, consistent with the documented presence of savannah and desert grassland in the eastern Sahara (e.g., Hoelzmann et al., 2000; Ritchie and Haynes, 1987; Kuper and Kröpelin, 2006). After the AHP, during the Mid-Late Holocene aridification, rainfall diminished to less than 50 mm/yr (Nicoll, 2004; Kröpelin et al., 2008), and today this region receives less than 2 mm/yr. Given these yearly rainfall estimates, the hourly rainfall intensities reported here of 55–80 mm/h during episodes of fluvial activity would represent total rainfall delivery periods of 1–4 h before the AHP, 4–14 h during the AHP, and less than 1 h after the AHP. Although we cannot assess the duration of individual rainfall events, this nevertheless suggests that precipitation during the AHP either took place 3–4 times more frequently (if the events' duration did not change) or in events of 3–4 times

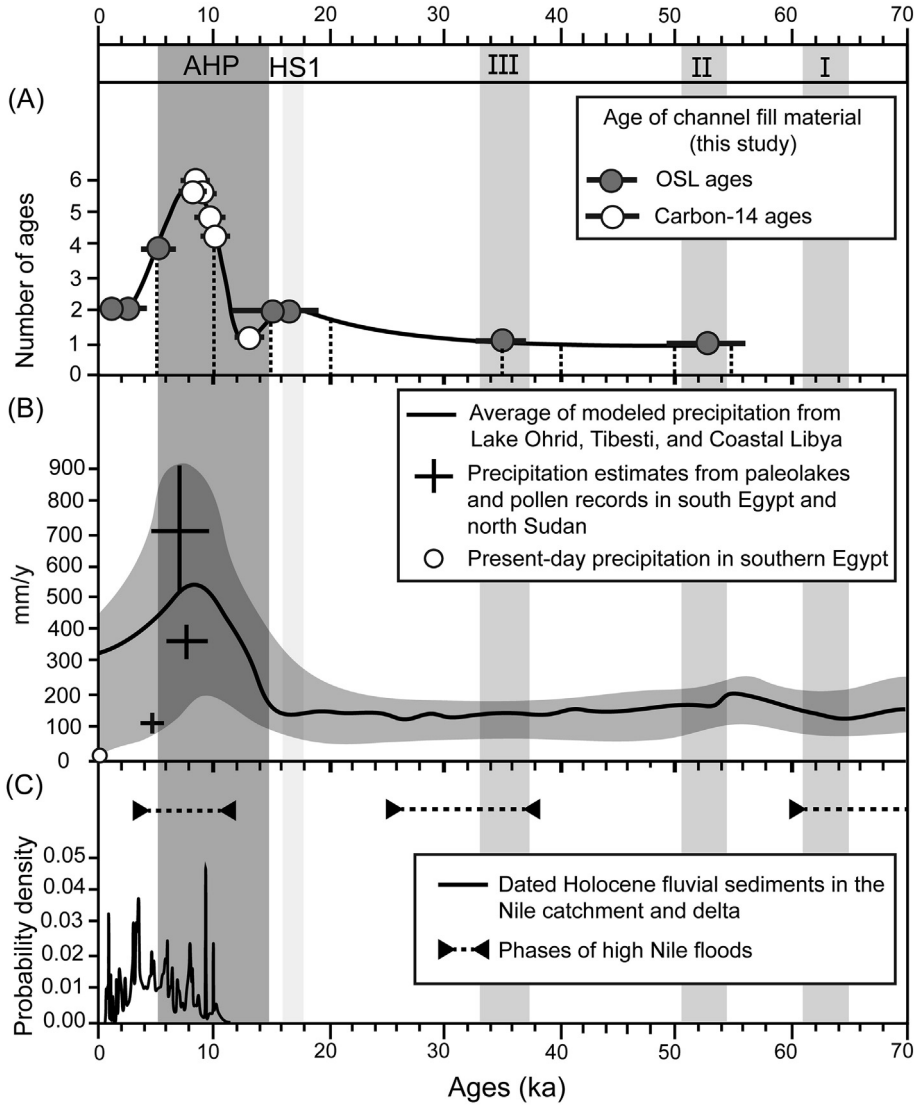

Fig. 6. Compilation of environmental proxies from the Sahara. (A) The number of ages reported from the fossil rivers studied here. The ages of the palaeorivers indicate six distinct phases during the past 53 ka. White dots represent calibrated ^{14}C dates, and gray dots indicate OSL ages. The distribution of the ages suggests an intense period of fluvial activity during the AHP. (B) Average of modeled and reconstructed mean annual precipitation over the past 70 ka. The modeled precipitation reported from Lake Ohrid (Wagner et al., 2019), and Tibesti and Coastal Libya (Blanchet et al., 2021). Reconstructed precipitation based on palaeolakes and pollen records has been plotted based on information reported from West Nubia Palaeolake Basin (Hoelzmann et al., 2000), Selima (Haynes et al., 1989), Bir Atrun and Oyo (Ritchie and Haynes, 1987), and Lake Yoa (Kröpelin et al., 2008). Present-day rainfall has been extracted from (https://weather-and-climate.com). (C) Reconstructed phases of high Nile floods over the past 70 ka (Williams et al., 2015), and the cumulative probability density function plots of the dated Holocene fluvial sediments from the Nile's catchment and delta (Macklin et al., 2015). Three wet periods (III, II, I) shaded by (light gray) were recorded by speleothems in Susah Cave, Libya (Hoffmann et al., 2016). The AHP is in a dark gray area (deMenocal et al., 2000).

longer duration. Insolation increase during the AHP is thought to have promoted higher temperature by up to 7.5 °C (deMenocal et al., 2000; Martrat et al., 2004). According to the Clausius-Clapeyron relation (Trenberth et al., 2003), such warming would enhance the atmosphere's water-holding capacity and MAP by 66%, much lower than our calculated factor of 3–4. Our results are thus more consistent with a "super" Clausius-Clapeyron (Lenderink and Meijgaard, 2008) scaling between temperature and precipitation, which would yield a ~2.7 fold increase in rainfall for the AHP warming of 7.5 °C. This excessive increase in rainfall during the AHP could have been linked to intense tropical summer monsoonal rainfall, sourced from the Mediterranean Sea, the Atlantic Ocean, and Indian Ocean (Hoelzmann et al., 2000; Kuper and Kröpelin, 2006; deMenocal et al., 2000; Shanahan et al., 2015). During the summer, the Saharan land surface may have been heated more efficiently than the adjacent Atlantic Ocean and the Mediterranean Sea, driving low pressure over the Sahara (deMenocal et al., 2000). This intense low pressure over the Sahara could have brought a significant inflow of moisture by wind, leading to intense seasonal rainfall during the summer (Hoelzmann et al., 2000; deMenocal et al., 2000).

Human occupation of the margins of the Nile in southern Egypt and northern Sudan began before ca. 25 ka BP and was associated with hyperarid conditions, which forced the limit of the Sahara desert ~400 km farther south than its current position; no settlements are documented in the deep Sahara (Kuper and Kröpelin, 2006; Vermeersch, 2002; Wendorf, 1968; Leplongeon, 2021, Fig. 7A; Movie S1). During the AHP, previous work has proposed that the climate perturbation drove settlements to disperse into the deep Sahara (Fig. 7 B; Kuper and Kröpelin, 2006) because of both enhanced monsoon rains, which favored milder savannah-like environments in the Sahara and hazardous and possibly marshy

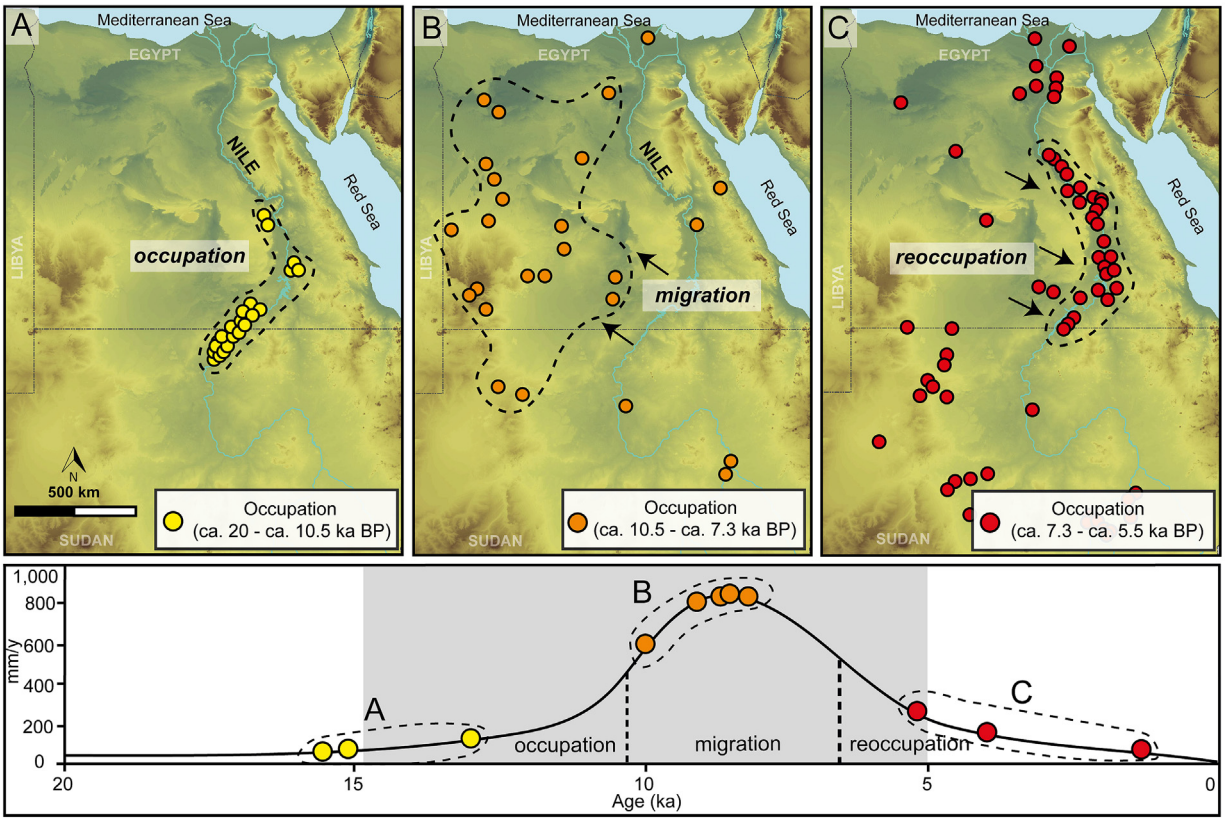

Fig. 7. Distribution of human settlements in the eastern Sahara over the Holocene epoch plotted from (Kuper and Kröpelin, 2006; Vermeersch, 2002; Vermeersch et al., 2015; Leplongeon, 2021). The curve represents the average of modeled and reconstructed precipitation rates, simplified from (Fig. 6 B). (A) The human settlements were concentrated along the Nile River Valley in southern Egypt and northern Sudan before ca. 10.5 ka BP because of Sahara's arid conditions as recorded by mean annual precipitation. This is consistent with the dearth of ages recorded by our study. (B) During the peak of AHP (ca. 10.5 – ca.7.3 ka BP), the mean annual precipitation had risen to the peak levels (up to 3–4 times more than before), transferring the hyper-arid conditions to savannah-like environments, reflecting hospitable regions in the deep Sahara for human settlements. This increase of mean annual precipitation and our estimates of intensity likely turned the Nile Valley into a hazardous place due to flood-related risks, driving people to migrate mainly to the west and northwestwards for roughly 3 ka. (C) Once the mean annual precipitation started to decline at ca. 7 ka BP, the populations reoccupied the Nile Valley because of the Sahara's arid conditions. Our reconstructions suggest fewer dates during the past 5 ka, reflecting the dramatic, strong, and drastic diminishing of humid conditions.

conditions along the Nile Valley in southern Egypt and northern Sudan due to increased fluvial activity (Kuper and Kröpelin, 2006; Movie S1). Our results demonstrate that rainfall activity magnified by a factor of 3–4 during the AHP (10.5–7.3 ka BP), are consistent with these observations and bring a quantitative estimate of the increase in flood-related risks for riparian populations. These flood-related risks might have turned some parts of southern Egypt and northern Sudan into hazardous places that resulted in settlement abandonment for nearly 3200 years. Flood-induced human migration likely occurred when increased precipitation and discharge raised the rivers' avulsion rates, driving large-scale flooding to partly or wholly immerse the Nile's marginal areas and floodplains. This scenario is, for instance, consistent with the recent catastrophic floods that cause millions of population displacements globally every year (Kakinuma et al., 2020). The link between environmental challenges and the dynamics of human populations is also consistent with the observation that the population returned along the Nile Valley corridor when it became more hospitable than the Sahara in response to the termination of the AHP and correlative aridification of the Sahara (Fig. 7 C; Kuper and Kröpelin, 2006; Nicoll, 2004; Macklin et al., 2015; Movie S1). Despite existing more hospitable places along the Nile Valley after the end of the AHP, Macklin et al. (2013) reported two phases of decreased Nile flows recorded by channel contractions in northern Sudan between ca. 4–3 ka BP and after 3 ka BP that were hazardous, causing settlements abandonment. Our chronologic data show that at least two palaeorivers were active after the AHP (ca. 5.2, 3.9, 1.1 ka BP); however, we could not notice any changes in human occupation. But catastrophic storms were mentioned in a broken stele in Karnak temple (~250 km north of the study area), describing the destruction of the Thebes region ca. 3.5 ka ago (Vandersleyen, 1967), reflecting that the floods after the AHP were hazardous, but to some extent, were manageable.

Supplementary data related to this article can be found at https://doi.org/10.1016/j.quascirev.2021.107200.

Global climate simulations and observations suggest that current global warming leads to greater evaporation rates and higher magnitude and frequency of floods and droughts (Coumou and Rahmstorf, 2012; Westra et al., 2013). Our results tell a narrative of a similar situation in the human past, a multimillennial experiment in human ecodynamics, which provides a pre-historical perspective on the current situation. Despite the challenges naturally inherent to estimating past climatic conditions, such palaeohydraulic reconstructions from the sedimentary record may represent essential tools for calibrating past and forward climate predictions.

Despite the uncertainties of reconstructing original river geometry (water depth and channel width) and grain size from preserved sediments (Paola and Borgman, 1991), several recent works demonstrate the potential of fossil rivers as archives of ancient precipitation rates, for instance, during the Palaeocene-Eocene Thermal Maximum (Chen et al., 2018; Shields et al., 2021) and

late Quaternary climatic oscillations (Litty et al., 2016). Our results, therefore, add to the growing recognition of the importance of sedimentary records of fossil rivers as a promising quantitative tool to assess past palaeohydraulics perturbations in deserts.

5. Conclusions

Based on the analysis of preserved fossil river channels, this work brings a new chronological and environmental context for the eastern Sahara desert and its human occupation and provides quantitative information about palaeo-rainfall intensity during the past pluvial periods of the Quaternary in this hyperarid part of Earth. Our palaeo-precipitation estimates associated with the new ages suggest that heavy rainfall events were characteristically in the range of 55–80 mm/h during phases of sediment transport over the past 53 ka BP. When paired with previous annual rainfall estimates, we find that such rainfall intensities likely occurred 3–4 times more frequently during the AHP. The ensuing climatic perturbation may have turned some parts of the Nile River Valley in southern Egypt and northern Sudan into a hazardous and inhospitable place for human occupation between 10.2 and 7.2 ka BP because of the increased risk of flooding. Our reconstructions, alongside the archeological data, exemplify climatic challenges to populations, highlighting the interactions between global warming, aberrations in heavy rainfall events, and their impact on humans.

Declaration of competing interest

The authors declare that they have no known competing financial interests or personal relationships that could have appeared to influence the work reported in this paper.

Acknowledgments

This research was funded by a Swiss Confederation Ph.D. grant (Nr: 2017.1006) to A.S.Z. Travel, fieldwork, and laboratory analyses were sponsored by Ernst et Lucie Schmidheiny Foundation and Augustin Lombard fellowships to A.S.Z. We thank Maxine Kleindienst for enlightening discussions about the pottery industry in the region during the Holocene epoch. Also, we thank Timothée Sassolas-Serrayet for discussing Hack's law. The manuscript has benefited from the constructive reviews of Giovanni Zanchetta, Martin Williams, and an anonymous reviewer.

Author contributions

Abdallah S. Zaki and Sébastien Castelltort conceived the scientific question, designed and performed the analysis, and wrote the manuscript. Georgina E. King, Frédéric Herman., and Negar Haghipour supervised OSL and ^{14}C dating. Robert Giegengack, Sanjeev Gupta, Mathieu Schuster, and Stephen E. Watkins assisted with regional geology, anthropology, and the interpretation of fluvial deposits. Abdallah S. Zaki led the collection of field data with the assistance of Hossam Khairy, Salah Ahmed, Mostafa El-Wakil, Saleh A. Eltayeb. All authors contributed to the discussion and interpretation of the data and writing of the manuscript. They also approved the final version.

Appendix A. Supplementary data

Supplementary data to this article can be found online at https://doi.org/10.1016/j.quascirev.2021.107200.

References

Abotalib, A.Z., Sultan, M., ElKadiri, 2016. Groundwater processes in Saharan Africa: implications for landscape evolution in arid environments. Earth Sci. Rev. 156, 108–136. https://doi.org/10.1016/j.earscirev.2016.03.004.

Abotalib, A.Z., Sultan, M., Jimenez, G., Crossey, L., Karlstrom, K., Forman, S., Krishnamurthy, R.V., Elkadiri, R., Polyak, V., 2019. Complexity of Saharan paleoclimate reconstruction and implications for modern human migration. Earth Planet Sci. Lett. 508, 74–84. https://doi.org/10.1016/J.EPSL.2018.12.015.

American Meteorological Society, 2012. Glossary of Meteorology. http://glossary.ametsoc.org/wiki/Rain.

Balescu, S., Lamothe, M., Mercier, N., Huot, S., Balteanu, D., Billard, A., Hus, J., 2003. Luminescence chronology of Pleistocene loess deposits from Romania: testing methods of age correction for anomalous fading in alkali feldspars. Quat. Sci. Rev. 22 (10–13), 967–973. https://doi.org/10.1016/S0277-3791(03)00056-8.

Bar-Matthews, M., Ayalon, A., Gilmour, M., Matthews, A., Hawkesworth, C.J., 2003. Sea–land oxygen isotopic relationships from planktonic foraminifera and speleothems in the Eastern Mediterranean region and their implication for paleorainfall during interglacial intervals. Geochem. Cosmochim. Acta 67 (17), 3181–3199. https://doi.org/10.1016/S0016-7037(02)01031-1.

Bell, W.T., 1980. Alpha attenuation in quartz grains for thermoluminescence dating. Anc. TL 12, 4–8.

Berg, P., Moseley, C., Haerter, J.O., 2013. Strong increase in convective precipitation in response to higher temperatures. Nat. Geosci. 6, 181–185. https://doi.org/10.1038/ngeo1731.

Berger, A., Loutre, M.F., 1991. Insolation values for the climate of the last 10 millions years. Quat. Sci. Rev. 10, 297–317. https://doi.org/10.1016/0277-3791(91)90033-Q.

Blanchet, C.L., Osborne, A.H., Tjallingii, R., Ehrmann, W., Friedrich, T., Timmermann, A., Bruckmann, W., Frank, M., 2021. Drivers of river reactivation in North Africa during the last glacial cycle. Nat. Geosci. 14, 97–103. https://doi.org/10.1038/s41561-020-00671-3.

Bronk Ramsey, C., 2009. Bayesian analysis of radiocarbon dates. Radiocarbon 51 (1), 337–360. https://doi.org/10.1017/S0033822200033865.

Brookes, H.E., Stensrud, D.J., 2000. Climatology of heavy rain events in the United States from hourly precipitation observation. Mon. Weather Rev. 128, 1194–1201. https://doi.org/10.1175/1520-0493(2000)128<1194:COHREI>2.0.CO2.

Chen, C., Guerit, L., Foreman, B.Z., et al., 2018. Estimating regional flood discharge during Palaeocene-Eocene global warming. Sci. Rep. 8, 13391. https://doi.org/10.1038/s41598-018-31076-3.

Church, M., Rood, K., 1983. Catalogue of Alluvial River Channel Regime Data. The University of British Columbia, Department of Geography, Vancouver, p. 99.

Collins, J.A., Govin, A., Mulitza, S., Heslop, D., Zabel, M., Hartmann, J., Rohl, U., Wefer, G., 2013. Abrupt shifts of the Sahara–Sahel boundary during Heinrich stadials. Clim. Past. 9, 1181–1191. https://doi.org/10.5194/cp-9-1181-2013.

Coumou, D., Rahmstorf, S., 2012. A decade of weather extremes. Nat. Clim. Change 2, 491–496. https://doi.org/10.1038/nclimate1452.

Damnati, B., 2000. Holocene lake records in the northern hemisphere of Africa. J. Afr. Earth Sci. 31 (2), 253–262. https://doi.org/10.1016/S0899-5362(00)00089-0.

deMenocal, P., Ortiz, J., Guilderson, T., Adkins, J., Sarnthein, M., Baker, L., Yarusinky, M., 2000. Abrupt onset and termination of the African humid period. Quat. Sci. Rev. 19. https://doi.org/10.1016/s0277-3791(99)00081-5, 347–36.

Drake, N.A., Blench, R.M., Armitage, S.J., Bristow, C.S., White, K.H., 2011. Ancient watercourses and biogeography of the Sahara explain the peopling of the desert. Proc. Natl. Acad. Sci. U.S.A. 108, 458–462. https://doi.org/10.1073/pnas.1012231108.

Duller, R.A., Whittaker, A., Swinehart, J.B., Armitage, J.J., Sinclair, H.D., Bair, A., Allen, P.A., 2012. Abrupt landscape change post–6 Ma on the central Great Plains, USA. Geology 40 (10), 871–874. https://doi.org/10.1130/G32919.1.

Durcan, J.A., King, G.E., Duller, G.A.T., 2015. DRAC: dose rate and age calculator for trapped charge dating. Quat. Geochronol. 28, 54–61. https://doi.org/10.1016/j.quageo.2015.03.012, 2015.

Fleitmann, D., Burns, S.J., Pekala, M., Mangini, A., Al-Subbary, A., Al-Aowah, M., Kramers, J., Matter, A., 2011. Holocene and Pleistocene pluvial periods in Yemen, southern Arabia. Quat. Sci. Rev. 30 (7–8), 783–787. https://doi.org/10.1016/j.quascirev.2011.01.004.

Foucault, A., Stanley, D., 1989. Late Quaternary palaeoclimatic oscillations in East Africa recorded by heavy minerals in the Nile delta. Nature 339, 44–46. https://doi.org/10.1038/339044a0, 1989.

Gasse, F., Chalié, F., Vincens, A., Williams, M.A.J., Williamson, D., 2008. Climatic patterns inequatorial and southern Africa from 30,000 to 10,000 years ago reconstructed fromterrestrial and near-shore proxy data. Quat. Sci. Rev. 27, 2316–2340. https://doi.org/10.1016/j.quascirev.2008.08.027.

Giegengack, R.F., Zaki, A.S., 2017. Inverted topographic features, now submerged beneath the water of Lake Nasser, document a morphostratigraphic sequence of high-amplitude late-Pleistocene climate oscillation in Egyptian Nubia. J. Afr. Earth Sci. 136, 176–187. https://doi.org/10.1016/j.jafrearsci.2017.06.027.

Guerin, G., Mercier, N., Adamiec, G., 2011. Dose-rate conversion factors. Anc. TL 29 (1), 5–8.

Hack, J.T., 1957. Studies of longitudinal stream profiles in Virginia and Maryland. U. S. Geol. Surv. Prof. Pap. B 294, 1–97.

Hamdan, M.A., Lucarini, G., 2013. Holocene palaeoenvironmental,

palaeoclimaticand geoarchaeological significance of the Sheikh El-Obeiyid area (Farafra Oasis,Egypt). Quat. Int. 302, 154–168.
Hamdan, A.H., Brook, G.A., 2015. Timing and characteristics of Late Pleistocene and Holocene wetter periods in the Eastern Desert and Sinai of Egypt, based on ^{14}C dating and stable isotope analysis of spring tufa deposits. Quat. Sci. Rev. 130, 168–188. https://doi.org/10.1016/j.quascirev.2015.09.011.
Haynes, C.V., Eyles, C.H., Pavlish, L.A., Ritchie, J.C., Rybak, M., 1989. Holocene palaeoecology of the eastern Sahara; Selima oasis. Quat. Sci. Rev. 8, 109–136. https://doi.org/10.1016/0277-3791(89)90001-2.
Hoelzmann, P., Kruse, H., Rottinger, F., 2000. Precipitation estimates for the eastern Saharan palaeomonsoon based on a water balance model of the West Nubian Palaeolake Basin. Global Planet. Change 26 (1–2), 105–120. https://doi.org/10.1016/S0921-8181(00)00038-2.
Hoffmann, D.L., Rogerson, M., Spotl, C., Luetscher, M., Vance, D., Osborne, A.H., Fello, N.M., Moseley, G.E., 2016. Timing and causes of North African wet phases during the last glacial perios and implications for modern human migration. Sci. Rep. 6, 36367. https://doi.org/10.1038/srep36367.
Huntley, D.J., Brail, M.R., 1997. The K content of K-feldspars being measured in optical dating or in thermoluminescence dating. Anc. TL. 15, 11–13.
Kakinuma, K., Puma, M.J., Hirabayashi, Y., Tanoue, M., 2020. Flood-induced population displacements in the world. Environ. Res. Lett. 15, 124029. https://doi.org/10.1088/1748-9326/abc586.
Kleindienst, M.R., Blackwell, B.A.B., Skinner, A.R., Churcher, C.S., Kieniewicz, J.M., Smith, J.R., Wise, N.L., Long, R.A., Deely, A.E., Blickstein, J.I.B., Chen, K.K.L., Huang, A., Kim, M.Q.D., 2016. Assessing long-term habitability at an eastern Sahara oasis: ESR dating of molluscs and herbivore teeth at Dakhleh Oasis, Egypt. Quat. Int. 408 (B), 106–120. https://doi.org/10.1016/j.quaint.2015.11.045.
Komada, T., Anderson, M.R., Dorfmeier, C.L., 2008. Carbonate removal from coastal sediments for the determination of organic carbon and its isotopic signatures, $\delta^{13}C$ and $\Delta^{14}C$: comparison of fumigation and direct acidification by hydrochloric acid. Limnol Oceanogr. Methods 6, 254–262. https://doi.org/10.4319/lom.2008.6.254.
Kröpelin, S., Verschuren, D., Lezine, A., Eggermont, H., Cocquyt, C., Francus, P., Cazet, J.P., Fagot, M., Rumes, B., Russell, J.M., Daruis, F., Conley, D.J., Schuster, M., Suchodoletz, H.V., Engstorm, D.R., 2008. Climate-driven ecosystem succession in the Sahara: the past 6000 years. Science 320 (5877), 765–768. https://doi.org/10.1126/science.1154913.
Kuper, R., Kropelin, S., 2006. Climate-controlled Holocene occupation in the Sahara: motor of Africa's evolution. Science 303 (5788), 803–807. https://doi.org/10.1126/science.1130989.
Lenderink, G., Meijgaard, E.V., 2008. Increase in hourly precipitation extremes beyond expectations from temperature changes. Nat. Geosci. 1, 511–514. https://doi.org/10.1038/ngeo262.
Leplongeon, A., 2021. The main Nile Valley at the end of the Pleistocene (28–15 ka): dispersal corridor or environmental refugium? Front. Earth Sci. 8, 607183. https://doi.org/10.3389/feart.2020.607183.
Litty, C., Duller, R., Schlunegger, F., 2016. Paleohydraulic reconstruction of a 40 ka-old terrace sequence implies that water discharge was larger than today. E*arth Surf. Process. Landforms* 41, 884–898. https://doi.org/10.1002/esp.3872.
Macklin, M.G., Toonen, W.H.J., Woodward, J.C., Williams, M., Flaux, C., Marriner, N., Nicoll, K., Verstraeten, G., Spencer, N., Welsby, D., 2015. A new model of river dynamics, hydroclimatic change and human settlement in the Nile Valley derived from meta-analysis of the Holocene fluvial archive. Quat. Sci. Rev. 130, 109–123. https://doi.org/10.1016/j.quascirev.2015.09.024.
Macklin, M.G., Woodward, J.C., Welsby, D.A., Duller, G.A.T., Williams, F.M., Williams, M.A.J., 2013. Reach-scale river dynamics moderate the impact of rapid Holocene climate change on floodwater farming in the desert Nile. Geology 41, 695–698.
Manning, K., Timpson, A., 2014. The demographic response to Holocene climate change in the Sahara. Quat. Sci. Rev. 101, 28–35. https://doi.org/10.1016/j.quascirev.2014.07.003, 2014.
Martrat, B., Frimalt, J.O., Lopez-Martines, C., Cacho, I., Sierro, F.J., Flores, J.A., Zahn, R., Canals, M., Curtis, J.H., Hodell, D.A., 2004. Abrupt temperature changes in the western Mediterranean over the past 250,000 years. Science 306 (5702), 1762–1765. https://doi.org/10.1126/science.1101706.
Mawson, R., Williams, M., 1984. A wetter climate in eastern Sudan 2,000 years ago? Nature 309 (5963), 49–51.
Mejdahl, V., 1979. Thermoluminescence dating: beta-dose attenuation in quartz grains. Archaeometry 21, 61–72.
Nicoll, K., 2004. Recent environmental change and prehistoric human activity in Egypt and Northern Sudan. Quat. Sci. Rev. 23, 561–580. https://doi.org/10.1016/j.quascirev.2003.10.004.
Palchan, D., Torfstien, A., 2019. A drop in Sahara dust fluxes records the northern limits of the African Humid Period. Nat. Commun. 3803. https://doi.org/10.1038/s41467-019-11701-z.
Paola, C., Borgman, L., 1991. Reconstructing random topography from preserved stratification. Sedimentology 38, 553–565. https://doi.org/10.1111/j.1365-3091.1991.tb01008.x.
Pausata, F.S.R., Gaetani, M., Messori, G., Berg, A., Maia de Souza, D., Sage, R.F., deMenocal, P.B., 2020. The greening of the Sahara: past changes and futureimplications. One Earth 2, 235e250. https://doi.org/10.1016/j.oneear.2020.03.002.
Prescott, J.R., Hutton, J.T., 1994. Cosmic ray contributions to dose rates for luminescence and ESR dating: large depths and long-term time variations. Radiat. Meas. 23, 497–500. https://doi.org/10.1016/1350-4487(94)90086-8.
Reimer, P.J., et al., 2013. IntCal13 and Marine13 radiocarbon age calibration curves 0–50,000 years cal bp. Radiocarbon 55, 1869–1887. https://doi.org/10.2458/azu_js_rc.55.16947, 2009.
Ritchie, J.C., Haynes, C.V., 1987. Holocene vegetation zonation in the eastern Sahara. Nature 330 (6149), 645–647. https://doi.org/10.1038/330645a0.
Sassolas-Serrayet, T., Cattin, R., Ferry, M., 2018. The shape of watersheds. Nat. Commun. 3791. https://doi.org/10.1038/s41467-018-06210-4.
Schuster, M., Roquin, C., Duringer, P., Brunet, M., Caugy, M., Fontugne, M., Mackaye, H.T., Vignaud, P., Ghienne, J., 2005. Holocene lake mega-Chad palaeoshorelines from space. Quat. Sci. Rev. 24 (16–17), 1821–1827. https://doi.org/10.1016/j.quascirev.2005.02.001.
Shanahan, T., McKay, N., Hughen, K., et al., 2015. The time-transgressive termination of the African humid period. Nat. Geosci. 8, 140–144. https://doi.org/10.1038/ngeo2329.
Shields, C.A., Kiehl, J.T., Rush, W.D., Rothstein, M., Snyder, M.A., 2021. Atmospheric rivers in high-resolution simulations of the Paleocene Eocene thermal Maximum (PETM). Palaeogeogr. Palaeoclimatol. Palaeoecol. https://doi.org/10.1016/j. palaeo.2021.110293.
Tierney, J.E., Pausata, F.S.R., deMenocal, P.B., 2017. Rainfall regimes of the green Sahara. Sci. Adv. 1, e1601503. https://doi.org/10.1126/sciadv.1601503.
Trampush, S.M., Huzurbazar, S., McElroy, B., 2014. Empirical assessment of theory for bankfull characteristics of alluvial channels. Water Resour. Res. 50, 9211–9220. https://doi.org/10.1002/2014wr015597.
Trenberth, K.E., Dai, A., Rasmussen, R.M., Parsons, D.B., 2003. The changing character of precipitation. Bull. Am. Meteorol. Soc. 84, 1205–1217. https://doi.org/10.1175/BAMS-84-9-1205.
Trenberth, S.M., Zhang, Y., Gehne, M., 2017. Intermittency in precipitation: duration, frequency, intensity, and amounts using hourly data. J. Hydrometeorol. 18, 1393–1412. https://doi.org/10.1175/JHM-D-16-0263.1.
Vandersleyen, C., 1967. Une tempête sous le règne d'Amosis. Revue d'Égyptologie 19, 123–159.
Vermeersch, P.M., 2002. Palaeolithic Quarrying Sites in Upper and Middle Egypt. Katholieke Universiteit Leuven, Leuven, p. 365.
Vermeersch, P.M., Linseele, V., Marinova, E., Neer, W.V., Moeyersons, J., Rethemyer, J., 2015. Early and middle Holocene human occupation of the Egyptian eastern desert: Sodmein cave. Afr. Archaeol. Rev. 32, 465–503. https://doi.org/10.1007/s10437-015-9195-6.
Wagner, H., Vogel, A., Francke, et al., 2019. Mediterranean winter rainfall in phase with African monsoons during the past 1.36 million years. Nature 573, 256–260. https://doi.org/10.1038/s41586-019-1529-0.
Wendorf, F.A., 1968. The Prehistory of Nubia. Southern Methodist University, Dallas, pp. 954–995.
Westra, S., Alexander, L.V., Zwiers, F.W., 2013. Global increasing trends in annual maximum daily precipitation. J. Clim. 26, 3904–3918. https://doi.org/10.1175/JCLI-D-12-00502.1.
Williams, R.M.E., Irwin, R.P., Zimbelman, J.R., 2009. Evaluation of paleohydrologic models for terrestrial inverted channels: implications for application to Martian sinuous ridges. Geomorphology 107, 300–315. https://doi.org/10.1016/j.geomorph.2008.12.015.
Williams, M., 2019a. The sudd swamps and the white nile. In: The Nile Basin: Quaternary Geology, Geomorphology and Prehistoric Environments. Cambridge University Press, Cambridge, pp. 107–126. https://doi.org/10.1017/9781316831885.009.
Williams, M., 2019b. The Ugandan lake plateau. In: The Nile Basin: Quaternary Geology, Geomorphology and Prehistoric Environments. Cambridge University Press, Cambridge, pp. 97–106. https://doi.org/10.1017/9781316831885.008.
Williams, M.A.J., Duller, G.A.T., Williams, F.M., Macklin, M.G., Woodward, J.C., El Tom, O.A.M., Munro, R.N., El Hajaz, Y., Barrows, T.T., 2015. Causal links between Nile floods and eastern Mediterranean sapropel formation during the past 125 kyr confirmed by OSL and radiocarbon dating of Blue and White Nile sediments. Quat. Sci. Rev. 130, 89–108.
Woodward, J.C., Macklin, M.G., Fielding, L., Millar, I., Spencer, N., Welsby, D., Williams, M., 2015. Shifting sediment sources in the world's longest river: a strontium isotope record for the Holocene Nile. Quat. Sci. Rev. 130, 124–140.
Wolman, M.G.A., 1954. Method of sampling coarse river-bed material. EOS Trans. Am. Geophys. Union 35, 951–956.
Zaki, A.S., Giegengack, R., 2016. Inverted topography in the southeastern part of the Western Desert of Egypt. J. Afr. Earth Sci. 121, 56–61. https://doi.org/10.1016/j.jafrearsci.2016.05.020.
Zaki, A.S., Pain, C., Edgett, K.E., Giegengack, R., 2018. Inverted stream channels in the Western Desert of Egypt: synergistic remote, field observations and laboratory analysis on Earth with application to Mars. Icarus 309, 105–124. https://doi.org/10.1016/j.icarus.2018.03.001.
Zaki, A.S., Pain, C.F., Edgett, K.S., Castelltort, S., 2021. Global inventory of fluvial ridges on Earth and lessons applicable to Mars. Earth Sci. Rev. 2016 (103561). https://doi.org/10.1016/j.earscirev.2021.103561.